Journal of Magnetic Resonance 309 (2019) 106619

Contents lists available at ScienceDirect

Journal of Magnetic Resonance

journal homepage: www.elsevier.com/locate/jmr

Sequence for simultaneous measurement of long-limit diffusion and longitudinal relaxation in unilateral NMR

Oscar Sucre *, Corinne Rondeau-Mouro

Irstea, UR OPAALE, 17 avenue de Cucillé, CS 64427, F-35044 Rennes, France
Université Bretagne Loire, France

ARTICLE INFO

Article history:
Received 16 July 2019
Revised 8 October 2019
Accepted 9 October 2019
Available online 18 October 2019

Keywords:
Low-field NMR
Gaussian pulse
Saturation recovery
Diffusion
T_1

ABSTRACT

When unilateral NMR is employed with large gradients (20 T/m), measurements of T_1 using standard sequences become affected by Brownian motion of spins, particularly in samples with long spin-lattice relaxation times T_1 (>2000 ms) and a large diffusion coefficient D ($2*10^{-6}$ mm^2/ms). In light of this, a modified saturation sequence which we have called GAUSS-SR is proposed that allows direct measurement of both D and T_1 to be carried out subject to certain constraints. The evolution of M_z magnetization is the main phenomenon to be modeled. The sequence is composed of three main parts: (i) a saturation train designed to render the M_z profile in Gaussian form, (ii) a main delay where by the simultaneous effects of T_1 and D on this profile has been solved analytically and (iii) a detection train to ensure a good signal-to-noise ratio. An NMR-MOUSE was used to acquire the desired measurement through this sequence. By relying on the coherence of the longitudinal rather than the transverse magnetization component, the sequence successfully provides the long-limit value of the diffusion coefficient.

1. Introduction

The emergence of unilateral low-field NMR in oilfield characterization [1], polymer science [2] and porous media [3] has demonstrated the value of this technique as a tool to investigate various industrial and research processes [4]. Its open geometry allows NMR signals to be measured in large sample volumes that are external to the sensor. Moreover, further devices (some large) useful for on-line measurements can be accommodated, for quality control in tire production for example [5]. The price paid for this ease of use is, in many cases, an inherently large gradient $\boldsymbol{g}$ for the static field $\boldsymbol{B_0}$. This causes the signal to dephase in a way that can, however, be compensated by using a suitable detection scheme. Once processed, the data obtained has provided information, mainly on spin-lattice T_1 and spin-spin T_2 type relaxation times and on diffusion coefficients D, that has also aroused interest in the food industries [6].

For unilateral NMR, the well-known Carr-Purcell-Meimboom-Gil (CPMG) sequence is the standard approach when measuring T_2 and D in experiments of short duration [4]. In addition, this sequence of radiofrequency (RF) pulses is the usual detection scheme employed in unilateral spectrometry, producing Signal-to-Noise Ratio (SNR) values comparable to those of high field NMR [7]. Measurement of T_1 consists in recording the longitudinal component of magnetization M_z during a given evolution time. To prepare this component for evolution, it must be either inverted or saturated using Inversion Recovery (IR) or Saturation Recovery (SR) sequences [8]. When the static gradient g is not very high (below 10 T/m) and the sample T_1 is relatively short (100 ms), both IR and SR sequences yield the correct T_1 values in unilateral NMR. However, under certain conditions, both the diffusion of the signal-yielding spins and the admixture of relaxation modes can cause the IR and SR sequences to yield false T_1 values. While Duan et al. [9] have taken into account the off-resonance effects that arise when the preparation sequence is also a CPMG sequence, their model does not include the possible effects on T_1 of diffusion during evolution time. Elsewhere, Nestlé et al. [10] have succeeded in modeling the effects of diffusion for stray-field NMR under a particularly high gradient (59 T/m) but not for unilateral NMR. Their method is based on the hole-burning sequence to measure diffusion, also developed for stray fields [11]. The inclusion of spatial transport from diffusion in T_1 relaxation phenomena is well-established by the Bloch-Torrey equation [12]. It demonstrates that, in addition to longitudinal magnetization, it is necessary to consider diffusive motions when static magnetic field gradients are present.

Solving the evolution of magnetization under both phenomena enables the simultaneous measurement of both T_1 and D using a

* Corresponding author at: Irstea, UR OPAALE, 17 avenue de Cucillé, CS 64427, F-35044 Rennes, France.
E-mail address: osucre@hotmail.com (O. Sucre).

https://doi.org/10.1016/j.jmr.2019.106619
1090-7807/

single sequence in unilateral NMR. This paper presents one implementation of such a sequence using a MOUSE (MObile Universal Surface Explorer) NMR system (NMR-MOUSE), a widely-used unilateral low-field instrument [4]. The sequence has the following particular characteristics: (i) the on-resonance volume (sensitive volume) is subjected to a static gradient and (ii) the signal is detected by surface coils with an inherently low filling factor. The new pulse sequence, named GAUSS-SR (Gaussian Saturation Recovery), measures the z magnetization component M_z throughout the evolution time. The theoretical model developed for this evolution takes into account both off-resonance effects during the preparation and acquisition periods and diffusion effects during the evolution time. The proposed simultaneous measurement of both quantities in absolute terms is thus made possible.

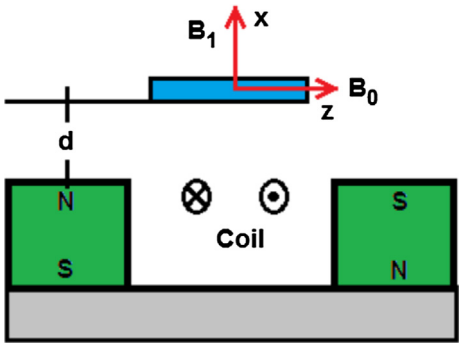

Fig. 2. Diagram of the NMR-MOUSE. Shown in blue, sensitive volume defined by the static and RF fields $\boldsymbol{B_0}$ and $\boldsymbol{B_1}$.

2. Theory of the GAUSS-SR sequence

The proposed GAUSS-SR sequence shown in Fig. 1 is composed of three main parts: (i) a saturation train, that is, a series of N2 aperiodic soft pulses separated by N2-1 delays, each of the latter having a different value. All pulses in the saturation train are applied with the same phase +x, thus generating a RF field at the sensitive volume. Each "soft" pulse is a segmentation made up of N1 pulses of a Gaussian pulse. Each segment is 2 μs in length. (ii) A main delay period, marked by a waiting time t_w and (iii) a detection train composed of a CPMG sequence with an acquisition window T_{ACQ} for *NE* pulses and echo time t_E. As is the usual practice, a recycling delay R_D is allowed to elapse between repetitions of the sequence. Because of the constraints imposed on the static and RF fields by unilateral NMR, the signals generated by many of the spins are produced under off-resonance conditions. Generally speaking, each pulse affects the spins with flip angle β. For spins that are sharply on-resonance only, this is equal to 180° for the duration of the application of the detection train.

There is no doubt that off-resonance conditions must be taken into account when modelling the effect of the GAUSS-SR sequence on magnetization. They are in fact determined in the first place by the operation of the NMR-MOUSE. A brief overview of the NMR-MOUSE is provided in Fig. 2. This contains a diagram of the device, together with vectors $\boldsymbol{B_0}$ and $\boldsymbol{B_1}$ for the static and the RF fields generated by the coil and the permanent magnets (in green) respectively. These vectors also show the respective directions of the z and x axes for the theory briefly developed here. The spatial dependency of the static field (which establishes the local Larmor frequency value $\omega_L = \gamma \boldsymbol{B_0}$) and the operation frequency ω_{rf} of the $\boldsymbol{B_1}$ field determine a sensitive volume (in blue) above the top of the sensor. The depth of measurement *d*, that is, the distance between the upper surface of the sensor and the sensitive volume, is 5 mm for all measurements presented here. Further details of the construction of the NMR-MOUSE can be found elsewhere [7].

The reference axis is set at the center of the sensitive volume: for x = 0, a location where the spins are sharply on resonance. This condition is also denoted by a local off-resonance frequency ω equals to 0, defined as $\omega = \omega_L - \omega_{rf}$. In the NMR-MOUSE, the gradient *g* of the static field is constant across the the sensitive volume. Therefore the x coordinate and ω are related to each other by the equation $\omega = \gamma g x$, making both the rotating frame and the expression of the Bloch equation associated with it space-dependent. The presence of the RF field $\boldsymbol{B_1}$ in the Bloch equation will be denoted by the angular velocity of precession in counterclockwise direction, defined as $\omega_1 = \gamma \boldsymbol{B_1}/2$.

The vector of magnetization $\mathbf{M} = [M_x, M_y, M_z]$ is represented by the complex number $M_+ = M_x + iM_y$ and M_z. The identity of the latter is kept apart due to its importance in investigating spin-lattice relaxation. Under the manipulation of coherence imposed by the GAUSS-SR sequence, the evolution of the couple [M+, Mz] takes place in two clearly different regimes, denoted as it follows

A) On-RF regime

When the RF pulses are on, the main interaction is produced by the tilting effect of the pulses. In this regime, the Bloch equation takes the following form [13] after having neglected the diffusion and relaxation terms:

$$\frac{\partial M_+}{\partial t} = -i\omega M_+ - i\omega_1(t) M_z \tag{1}$$

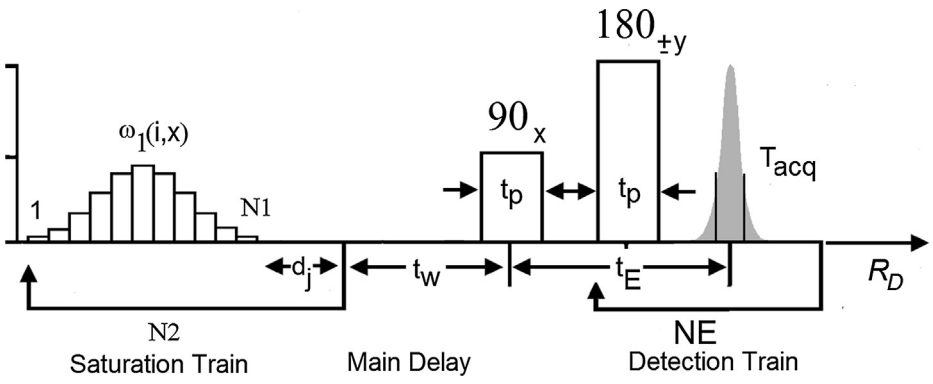

Fig. 1. GAUSS-SR Sequence for the measurement of T_1 and *D* in inhomogeneous fields. *N2* is the number of aperiodic soft pulses, made up of *N1* segments followed by d_j delays of different values. Together, these form the saturation train, followed by main delay t_w and a detection train to acquire the signal within an acquisition window T_{ACQ} (CPMG sequence made up of NE refocusing pulses of length t_p separated by the echo time t_E). Refocusing pulse tilt angles are 180° and 90° for spins that are sharply on resonance.

$$\frac{\partial M_z}{\partial t} = \omega_1(t)\mathbf{Im}(M_+) \tag{2}$$

B) Off-RF regime

When the RF pulses are off, the effects of relaxation and the spatial transport caused by diffusion are the main factors that govern the evolution of **M**. In this case a diffusion term has to be added, producing what is known as the Bloch-Torrey [12] equation in a space-dependent rotating frame as shown by Eqs. (3) and (4):

$$\frac{\partial M_+}{\partial t} = -i\omega M_+ + D\frac{\partial^2 M_+}{\partial x^2} - \frac{M_+}{T_2} \tag{3}$$

$$\frac{\partial M_z}{\partial t} = D\frac{\partial^2 M}{\partial t^2} - \left(\frac{M_z - M_0}{T_1}\right) \tag{4}$$

Naturally, only the x-dependency must be included in the diffusion term as this is the only direction against which the static field changes within the sensitive volume of the NMR-MOUSE. As a feature common to both regimes the off-resonance term $-i\omega M_+$ appears as a reminder of the strongly inhomogeneous character of the field. A key element in solving these equations becomes clear on examining Eq. (4), whereby the evolution of M_z is decoupled from that of the other **M** components, simplifying the corresponding theoretical treatment. In order to take advantage of this circumstance, the analysis for the evolution of the magnetization will be presented in the following order: Main Delay-Saturation Train-Detection Train.

1. Main delay

Following the application of the saturation train, a definitive profile $M_z(x)$ is assumed for the z magnetization component. In accordance with the assumed basis for Eqs. (1) and (2), the quantum description of the magnetization can be expressed using the spherical basis $\{I_+, I_-, I_z\}$. Because of its enclosed nature, when it is used to express the transfers described above this basis lends itself to model the effect of the pulses on the off-resonance spins. The shape of the profile can be calculated from the collective effects of the saturation train on the spin population. These effects are produced by a rather complicated coherence transfer between the populations of states $\{I_+, I_-, I_z\}$. At this point we can assume that such a profile exists and is described by a Gaussian bell around the center of the sensitive volume. Due to its suitability, further theoretical description will be refered from the off-resonance frequency ω.

One of the two main assumptions made in this research can be now introduced. First, the longitudinal magnetization should have the following form at the beginning of the main delay:

$$M_z(\omega) = M_0\left(1 - e^{-\omega^2/2\omega_A{}^2}\right) \tag{5}$$

whereby the quantity ω_A expressed in Hz is related to half the bandwidth of the Gaussian bell f_A by $\omega_A = 2\pi f_A$, and M_0 is the magnetization of the sample in equilibrium. The immediate goal in this subsection is to obtain the magnetization profile after the main delay has elapsed, that is, Mz (t_W, ω). Of course, Mz (0, ω) corresponds to the function of Eq. (5).

Eq. (4) provides the pathway to find Mz (t_w, x). Due to the decoupling of M_Z from the evolution of the other magnetization components, the solution can simply be written as [14]:

$$M_z(x, t_w) = M_0\left[1 - e^{-\frac{t_w}{T_1}}\int ds\, f(s)\,\frac{e^{-(x-s)^2/(4Dt_w)}}{\sqrt{4\pi D t_w}}\right]$$

whereby $f(s)$ is a function related to the initial profile $M_z(s)$ by $f(s) = M_z(s)/M_0 + 1$. If the coordinate x is now shifted to the off-resonance frequency ω, the last expression becomes:

$$M_z(\omega, t_w) = M_o\left[1 - e^{-t_w/T_1}\int d\omega_s\, f(\omega_s)\,\frac{e^{-(\omega-\omega_s)^2/2\omega_D^2}}{\sqrt{2\pi}\omega_D}\right] \tag{6}$$

which also includes the squared mean-free path of the spins after they have diffused during the main delay in units of radial frequency $\omega_D^2 = 2Dt_w\Upsilon^2 g^2$. After substituting $f(\omega_S)$ by the function given in Eq. (5), evaluation of Eq. (6) promptly yields Eq. (7):

$$M_z(\omega, t_w) = M_o\left[1 - \exp\left(-\frac{t_w}{T_1}\right)\exp\left(\frac{-\omega^2}{2(\omega_A^2 + \omega_D^2)}\right)\frac{\omega_A}{\sqrt{\omega_A^2 + \omega_D^2}}\right] \tag{7}$$

As a result, for a given slice with off-resonance frequency ω, Eq. (7) describes not only how the z magnetization component increases locally as a result of the spin-lattice relaxation but also how diffusive motion causes it to drift away from the initially-saturated slice. These two effects occur simultaneously. The subsequent detection procedure is applied over this broadening slice. However, in order to understand how such a slice can yield a detectable signal, it is important to see how the saturation train renders the $M_z(\omega)$ profile in the assumed Gaussian shape.

2. Saturation train

The goal of the saturation train (Fig. 1) is to saturate the spin population, that is means to dephase the local value of the z magnetization component so thoroughly that any attempt to measure it immediately thereafter will yield no signal. This is caused by all coherence pathways that have collapsed onto the I_z state at the end of the saturation train. As shown in Fig. 1, the saturation train consists of a series of *N2* aperiodic soft pulses with a 90° tilt angle and interspersed by *N2-1* delays. From the outset of this research it was clear that a saturated profile in Gaussian form would be advantageous in this regard due to the inherent properties of diffusion. In effect, the profile would remain strictly Gaussian during the whole main delay, facilitating the corresponding mathematical description of the phenomena. Bailes and Bryant's theory, which gives the first-order solutions of Eqs. (1) and (2), predicts that the magnetization will be supplied after the RF regime by the Fourier transform of the RF pulse [8], together with a phase term directly proportional to the static gradient. In that circumstance, application of a Gaussian soft pulse will suffice to obtain the desired Gaussian profile. Two practical constraints however make such an idea impossible to implement. First, due to the hardware limit, no segment of the RF pulse with constant amplitude can be smaller than 2 μs. Second, each pulse in the train must be a 90° pulse, thus reaching a tilt-angle range that lies well beyond the values considered by that theory. Despite those initial obstacles, it will be shown that careful adjustment of the six intertwined delays d_j makes possible to achieve such a profile with satisfactory accuracy.

A Gaussian bell with a half bandwidth f_A was taken as the objective function. The saturated train is composed of N2 RF soft pulses. Each soft pulse is the approximation, with N1 segments, of the objective function converted to the time domain. Calculations for the delays d_j have been carried out for two different saturation trains by selecting an f_A equal to 36 kHz for the first and 80 kHz for the second. Segmentation of the Gaussian bell occurs at N1 = 11 or 5 respectively. Fig. 3 illustrates the soft pulse segmented at N1 = 11. Half of the objective function bandwidth in the time domain is thus 4.4 μs (1/2π*36 kHz). The vector of amplitudes

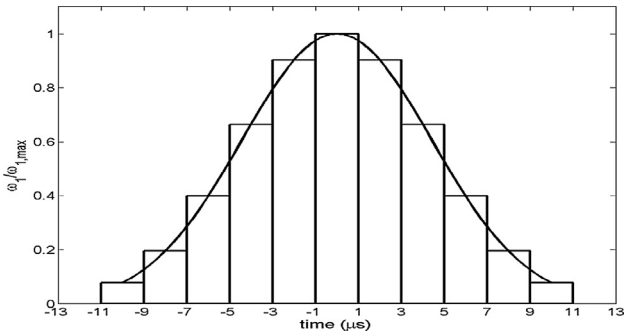

Fig. 3. 90° soft pulses of the N1 segments forming the saturation train. Continuous line indicates the approximated Gaussian bell (N1 = 11 for a half bandwidth of 4.4 μs).

ω_1, for both sequences and normalized to the central lobe, is presented in the Table 1.

Either when programming the saturation train simulation or when adjusting the attenuation in the pulse-shaping electronics, each vector of amplitudes must be scaled to make the corresponding tilt angle 90°. This is a task that poses no difficulties in any of the contexts mentioned. However, the adjustment of the delays d_j requires a far more careful approach. Indeed, their values must be such that the final effect of the saturation train resemble, as much as possible, the proposed objective function f(ω). If that final effect is labeled by the profile g(ω,d_j), where j={1,. . .,N2} and there is a long R_D (the magnetization vector should be in equilibrium at the beginning of the saturation train), the following matrix operation allows us to calculate g(ω,d_j):

$$g(\omega, d_j) = \left\{ \prod_{j=1}^{N2} \mathbf{L}(d_j)\mathbf{P}_j(\omega) \begin{bmatrix} 0 \\ 0 \\ 1 \end{bmatrix} \right\}_Z \tag{8}$$

whereby $L(d_j)$ and $P_j(\omega)$ are the rotation matrices associated with the free-precession periods and the RF soft pulses respectively. The former corresponds to the off-RF regime, where the evolutions of M_+ and Mz decouple, although the effects of diffusion are too minimal to require consideration given the short mean-free paths corresponding to the delays d_j. Therefore, L(dj) takes the form of a rotation matrix around the z-axis.

$$\mathbf{L}(d_i) = \begin{bmatrix} e^{-id_i\omega} & 0 & 0 \\ 0 & e^{id_i\omega} & 0 \\ 0 & 0 & 1 \end{bmatrix} \tag{9}$$

The minus sign in the exponent for the I_+ state and the plus sign for I_- are consequences of the counterclockwise rotation of protons. On the other hand, the rotation matrix for soft pulses $P_j(\omega)$ can be constructed from the combination of several rotation matrices R(ω, ω_1(i), Δt) for each of the N1 pulses of constant amplitude ω_1(i) that are tilting the magnetization exposed to an off-resonance frequency of ω during a time lapse Δt. The concrete form of R(ω, ω_1(i), Δt) will be presented later in this paper. The effect of the single soft pulse can thus be written as:

$$P_j(\omega) = \prod_{i=1}^{N1} \mathbf{R}(\omega, \omega_1(i), \Delta t) \tag{10}$$

Execution of Eq. (8) using the definitions of Eqs. (9) and (10) was programmed using MATLAB scripts. An error function χ^2 was then calculated from the integration over the ω-axis of the squared difference between f(ω) and g(ω,dj):

$$\chi^2(d_j) = \int d\omega \left(f(\omega) - g(\omega, d_j)\right)^2 \tag{11}$$

The result is naturally a function that is solely dependent on the vector of delays d_j. The space of delays d_j was explored to find the minimum χ^2 while subjecting the generation of values in this six dimensional space to two constraints: (i) all values are multiple of 10 μs (ii) all delays must increment monotonically with j. These strategies make the exploration less costly in computational terms. A global minimum was then searched for each of the sequences examined, with the results presented in Table 2.

In carrying out this investigation, it is important to mention that, prior to calculating the error function χ^2, the final profile g (ω,dj) is convoluted by a transfer function with diffusion bandwidth f_0 = 10 KHz. This operation filters the high-frequency oscillations exhibited by the raw profile without changing the general shape of the profile.

Results from the search for the minimum χ^2 (N1 = 11) g(ω,dj), together with the related objective function f (ω/2π) are shown in Fig. 4 with solid and dashed lines respectively.

We present now the rotation matrix R(ω,ω_1(i), Δt). The precession frequency with which the spins evolve locally is $\Omega = \sqrt{\omega^2 + \omega_1^2}$ in the on-RF regime. Clearly the flip angle β corresponding to each time segment Δt (2 μs) that makes up the soft pulse equals Ω.Δt. Depending on the offset resonance ω and the RF field ω_1, the local spins are deflected by an effective RF field that leans from the x axis at angle θ in accordance with the relation sin θ = ω/Ω. R(ω,ω_1(i), Δt) can be expressed in the spherical basis as [15]:

$$\mathbf{R}(\omega_0, \omega_1, \Delta t) = \begin{bmatrix} \frac{\left(\cos\beta\left(1+\cos^2\theta\right)+\sin^2\theta\right)}{2} + i\sin\beta\cos\theta & (\cos\beta - 1)\sin^2\theta/2 & (-(1-\cos\beta)\sin\theta\cos\theta + i\sin\beta\sin\theta)/\sqrt{2} \\ (\cos\beta - 1)\sin^2\theta/2 & \left(\left(\cos\beta\left(1+\cos^2\theta\right)+\sin^2\theta\right)\right)/2 + i\sin\beta\cos\theta & ((1-\cos\beta)\sin\theta\cos\theta - i\sin\beta\sin\theta)/\sqrt{2} \\ (-(1-\cos\beta)\sin\theta\cos\theta + i\sin\beta\sin\theta)/\sqrt{2} & ((1-\cos\beta)\sin\theta\cos\theta - i\sin\beta\sin\theta)/\sqrt{2} & \cos\beta\sin^2\theta + \cos^2\theta \end{bmatrix}$$

This matrix was incorporated in the MATLAB script to execute Eq. (10) and from that point onwards, the evaluation of the error function χ^2 proceeds through Eq. (11).

Once the magnetization has been saturated and allowed to evolve for the duration of the main delay, it must then be detected. We therefore turn our attention to the detection train.

3. Detection train

As previously mentioned, the detection train establishes, in accordance with its sequence parameters, a sensitive slice that need not to coincide fully with the saturated slice. They can however both be described using the Gaussian bell, an assumption of central importance in this research. The magnetization at the end

Table 1
Vector of amplitudes ω_1 for the N1-segmented soft pulses normalized to the central lobe.

N1	A_{-5}	A_{-4}	A_{-3}	A_{-2}	A_{-1}	A_0	A_1	A_2	A_3	A_4	A_5
11	0.07	0.19	0.39	0.66	0.9	1	0.9	0.66	0.39	0.19	0.07
5	–	–	–	0.13	0.6	1	0.6	0.13	–	–	–

Table 2
Saturation train delays between discretized soft pulses of 11 and 5 segments (N1).

N1	$d_1(\mu s)$	$d_2(\mu s)$	$d_3(\mu s)$	$d_4(\mu s)$	$d_5(\mu s)$	$d_6(\mu s)$	f_A(kHz)
11	20	80	140	180	520	560	36
5	100	230	270	310	520	660	80

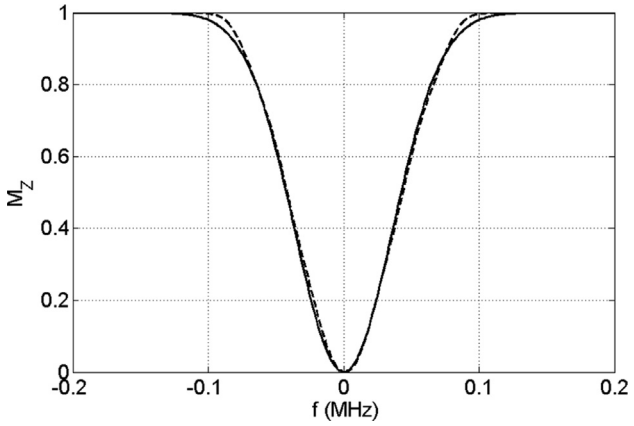

Fig. 4. Profile of Mz after a saturation train composed of seven (N2 = 7) aperiodic 90° spins and eleven segmented (N1 = 11) soft pulses (continuous line) and of the objective function, calculated from the Gaussian bell of half bandwidth f_A = 36 kHz (dashed line).

of the main delay, *Mz(ω,t_W)* in Eq. (7), can be considered to be the function representing the density of saturated spins around and within the sensitive slice. It also provides the initial spin density encountered at the beginning of the detection train. To detect the signal, it is definitely useful to employ a familiar expression from the theory of the CPMG sequence in inhomogeneous fields [16]. This is given by Eq. (12) as follows:

$$S(t_w) = \iint d\omega d\omega_1 \mathbf{f}(\omega,\omega_1)\omega_{RF}^2 m_{\infty,y}(\omega,\omega_1)F(\omega,Q) \tag{12}$$

whereby $\mathbf{f}(\omega, \omega_1)$ denotes the initial density of spins in the ω-ω_1 space, F(w,Q) is the frequency transfer function of the system as a detector of NMR signals and $m_{\infty,y}$ is the function that represents the frequency weighting imposed by the detection train.

Another simplifying hypothesis concerns the spatial inhomogeneity of ω_1. Though it clearly exists, it does so on a scale larger than the thickness of the sensitive slice [4]. We can thus assume that ω_1 is constant within the range of values for ω for which the integral of Eq. (12) is evaluated. The value ω_1 is of course determined by the pulse length through the relation $\omega_1 t_p = \pi/2$. In view of this simplification and the discussion previously devoted to Mz (ω,t_W), we can write:

$$S(t_w) = \frac{1}{2\pi\sqrt{\omega_B C}} \times \int d\omega M_z(\omega,t_w)\left[m_{\infty,y}(\omega,\omega_1,t_E,t_{90})F(\omega,Q)\otimes\frac{\sin(\omega T_{acq}/2)}{\omega T_{acq}/2}\right] \tag{13}$$

Convolution with Sinc function allows the effect of a finite acquisition window over the shape of the sensitive volume in the ω space to be correctly reproduced. Constants ω_B and C are adjoined for reasons that will become evident later. F(ω,Q, ω_{rf}) is in fact the squared transfer function of the tank circuit, which includes a quality factor Q. The direct expression of its dependency on the Larmor frequency is measured, not in the rotating frame ω, but in the laboratory frame $\omega + \omega_{rf}$ [17]

$$F(\omega,Q,\omega_{rf}) = 1/\left[1+\frac{(\omega+\omega_{rf})^2Q^2}{\omega_{rf}^2}\left(1-\frac{\omega_{rf}^2}{(\omega+\omega_{rf})^2}\right)^2\right] \tag{14}$$

The importance of function $m_{\infty,y}$ makes it worthy of an additional comment. One of the finest results from the theory of the CPMG sequence in highly inhomogeneous [16] fields is the proof of the existence of an effective rotational axis around which the spins revolve when exposed to this sequence. The projection of this asymptotic axis on the y-axis is the function $m_{\infty,y}$, which turns out to depend on the frequencies ω, ω_1 and the sequence parameters t_E and t_p as:

$$m_{\infty,y}(\omega,\omega_1) = \frac{\omega_1}{\Omega}\frac{\sin(\Omega t_p/2)\Omega}{1+\left[\frac{\Omega}{\omega_1}\sin(\omega t_E/2)\cot(\Omega t_{p/2})+\frac{\omega}{\omega_1}\cos(\omega t_E/2)\right]^2} \tag{15}$$

whereby Ω, again, denotes the precession frequency $\sqrt{\omega^2+\omega_1^2}$.

There are thus three functions $m_{\infty,y}$, F(w,Q, w_{RF}) and Sinc (ωT_{ACQ}) involved in the system's frequency response for the detection of NMR signals. Both physical (Q) and sequence-determined (T_{ACQ}, t_p, t_E) variables influence the final shape and thickness of the detection slice. The first-order thickness is inversely proportional to the pulse length $\Delta x = \pi/2\Upsilon g t_p$, however a more quantitative description is deemed necessary in order to apply the Gaussian approximation. This works smoothly, provided that the approximation taken is defined as:

$$e^{-\omega^2/2\omega_B^2} = \frac{1}{C}m_{\infty,y}(\omega,\omega_1,t_E,t_{90})F(\omega,Q,\omega_{rf})\otimes\frac{\sin(\omega T_{acq}/2)}{\omega T_{acq}/2} \tag{16}$$

in which the values of constants ω_B and C are simply those which make the last equation hold true. Defined as such, each of these constants also clearly relates to a physical property: ω_B is the half bandwidth of the detection slice and C is the area, within the ω space, of the function $m_{\infty,y}$*F(ω, Q, ω_{RF}) $\otimes$ Sinc($\omega T_{ACQ}/2$). In other words, C is a relative quantification of the number of spins the MOUSE is capable of detecting when the detection train is deployed.

To determine ω_B and C the convolution integral in Eq. (16) must be executed, an operation that can only be executed numerically. In the Material and methods section only ω_B, in kHz ($f_B = \omega_B/2\pi$) will be reported.

Therefore, with the approximation of Eq. (16), Eq. (13) promptly results in:

$$S(t_w) = M_o\left[1 - \frac{e^{-t_w/T_1}\omega_A}{\sqrt{\omega_A^2+\omega_B^2}}\frac{1}{\sqrt{2\pi}\omega_B}\int d\omega\ \exp\left(\frac{-\omega^2}{2(\omega_A^2+\omega_B^2)}\right)\exp\left(\frac{-\omega^2}{2\omega_B^2}\right)\right] \quad (17)$$

resulting in an integral that poses no difficulties in execution. If the radial frequencies ω_B and ω_A are now changed to their counterparts in Hz (f_A and f_B), the expression sought for the signal $S(t_w)$ comes out as:

$$S(t_w) = M_o\left[1 - \frac{e^{-t_w/T_1}f_A}{\sqrt{f_A^2+f_B^2+2D(\gamma g/2\pi)^2 t_W}}\right] \quad (18)$$

with f_A and f_B being constants determined solely by the sequence. They reflect the kinematics of multiple transfers of quantum coherences, which, as they are manipulated either by the saturation train or the detection train, establish the excited bandwidth in its effective value. To validate this new GAUSS-SR sequence, an experiment using a water sample was performed. The following section reports the results obtained.

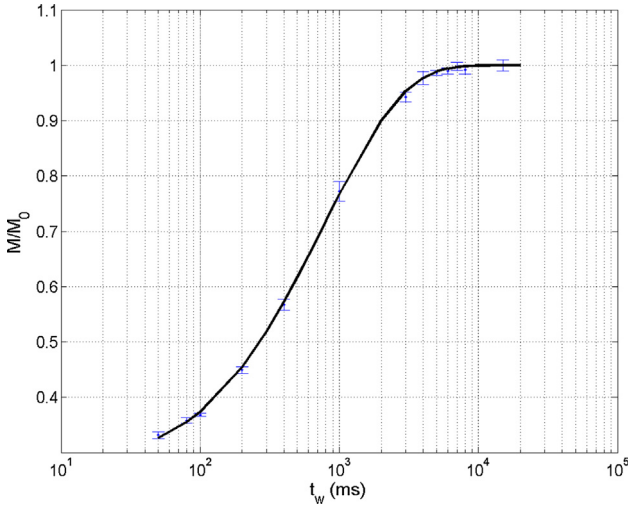

Fig. 5. Growth of M_z against the main delay t_w measured with the GAUSS-SR sequence. Sample: Distilled Water. T = 25C. Larmor frequency: 20 MHz.

3. Materials and methods

An NMR-MOUSE model PM5 (Magritek GmbH, Germany) equipped with a Kea electronic console was used. The Larmor frequency f_L was 20 MHz at the center of the sensitive volume and the given gradient $\Upsilon g/2\pi$ was at 996 kHz/mm. The depth of measurement (d) was 5 mm. This last condition is critical to the theory developed here. Indeed, if the value of d is diminished, the inhomogeneity of B_1 along the z and y axes increases and some of the simplifying assumptions discussed above cease to be valid. The sample comprised water distilled twice and kept in a sealed container during the experiment to eliminate any trace of paramagnetic oxygen and avoid further oxygen absorption. The GAUSS-SR sequence (Fig. 1) was applied to the water sample at 25 °C using 13 values for the delays t_W: 0.05, 0.08, 0.1, 0.2, 0.4, 1, 3, 4, 5, 6, 7, 8 and 15 s.

As for the sequence parameters (*N1*, *N2*, t_p, t_E, T_{ACQ}, R_d, *NE*) described in Fig. 1, their values, together with the number of repetitions *NS*, are reported in Table 3:

The quantity *ΔAtte* was the soft-pulse attenuation change with respect to the attenuation for the 90° rectangular pulse. It was simply calculated by assuming an area for the soft pulse equal to that of the rectangular 90° pulse. No phase-cycling was necessary for the saturation train. As for the detection train, the usual phase-cycling of the CPMG sequence was used.

As mentioned previously, the saturation train was adjusted to affect a Gaussian-shaped slice with half-bandwidth f_A of 34 kHz. f_B was calculated by executing Eq. (16) with the parameters in Table 1. It turned out to be 32 kHz.

4. Results and discussion

Measurements using the GAUSS-SR sequence on distilled water took 43 min to complete. The sequence was repeated six times to calculate the experimental uncertainty in the measurement. Fitting of experimental data (shown with error bars in Fig. 5) using Eq. (18), with M_0, T_1 and D as free parameters and f_A and f_B as fixed parameters yielded the adjusted curve of Fig. 5.

The distribution of values for the main delay t_W plays an important role in the implementation of the sequence. Values of t_w should be scattered mostly at the beginning and at the end of the saturation curve. The first set of values contains information about the T_1-dominated growth and the second set about the D-dominated growth. The strategy by which they are generated differs from that usually employed in the standard SR sequence (uniform distribution on the logarithmic scale). The fitting analysis gave final values for T_1 and D at 1700 ± 400 ms and 2.2 ± 0.5 * 10^{-6} mm^2/ms, respectively. These values match, within the parameters of experimental uncertainty, those reported in the literature [18].

Given the number of variables involved in Eq. (18), it can be assumed that considerable room for maneuver is available when designing the GAUSS-SR sequence. N1, N2 and the set of delays d_j determine f_A and t_p, t_E, and Q determines f_B. In fact there are certain constraints that must be complied with if the sequence is to be effective. A key consideration in designing the sequence is the half bandwidth of the affected slice, which can confidently be described by the quantity $\sqrt{f_A^2+f_B^2}$. The latter should be wide enough to guarantee a good SNR during acquisition but at the same time thin enough to allow the broadening effect of diffusion to have a marked effect on the growth of magnetization. This last constraint is expressed by the condition $\sqrt{2DT_1} * \frac{\gamma g}{2\pi} / \sqrt{f_A^2+f_B^2} \gg 1$. For example for the f_A and f_B values employed, this ratio reaches a value of 2. For the second sequence however, where N1 = 5 (f_A and f_B equal to 80 and 42 kHz, t_p = 7.5 μs), the ratio is just 1.1. In this latter sequence, the results are a poor reflection of the influence of diffusion on the longitudinal magnetization, introducing large uncertainties (data not shown) in the T_1 and D values when fitting Eq. (18). Therefore, only when appropriate sequence-parameter values are assigned will the translational behavior of the spins appear clearly in the data acquired.

A further constraint lies in the value of the acquisition window T_{acq}. Were too small the value selected (say 2 μsec), the *sinc* function would become wider, increasing the value of f_B (273 kHz)

Table 3
Sequence parameters for the GAUSS-SR Sequence.

N1	N2	t_p (μs)	t_E (μs)	T_{ACQ} (μs)	NS	Rd (s)	ΔAtte (dB)	NE
11	7	12	80	8	16	10	+4.4	128

through the convolution operation set out in Eq. (16). The ratio mentioned beforehand would no longer be greater than 1. This means that, in physical terms, we would be recording the signal from a slice that was wider than the polarized slice. In consequence, the diffused spins would still fall within the detection range after the main delay, thereby weakening the influence of diffusion. If, on the other hand, the window were to be set too large, the SNR ratio would worsen due to noise acquisition at those points where the signal was weak. Here, a value of T_{acq} of 75% of the pulse length worked well for our purpose.

It is important to look on the GAUSS-SR sequence as complementary to other sequences created to measure diffusion, not as a competitor. The reason for this lies in a profound conceptual difference between this and other sequences. For example, the Stimulated Spin Echo (STE) sequence [4] is an established method based on the manipulation of coherence in transverse magnetization. Using such a sequence, the value of D is obtained with typical diffusion times of 100 ms, a value that can be regarded as a short-time limit. By contrast, the GAUSS-SR sequence obtains diffusion values from the evolution of coherence on the longitudinal axis during the main delay with a diffusion time of the order of $3^{*}T_1$. The GAUSS-SR sequence therefore provides a very real route to acquisition of values for the long-time limit of D. The two sequences complement each other at picturing of the nature of diffusive motions measured by NMR.

5. Conclusion

The GAUSS-SR sequence is uniquely placed, as compared with other sequences, to measure simultaneously both the longitudinal relaxation time T_1 and the diffusion coefficient D. Meanwhile, parameters defining the three main components of the sequence (saturation train, main delay and detection train) have been calculated to allow the intended measurements to be carried out within the physical constraints of the NMR system (NMR-MOUSE gradient, tank-circuit quality, RF power delivered).

Such a sequence is useful for measurements using unilateral NMR systems where diffusion phenomena strongly affect the acquired data, i.e. using instruments with large gradients (at least 20 T/m) and samples with large D values (at least $2 * 10^{-6}$ mm^2/ms). This is of particular relevance for water in a heated sample: at 80 C, D becomes $6.6 * 10^{-6}$ mm^2/ms and $T_1 = 10^4$ ms [18]. Even when switching to the sequence parameter where N1 = 5 (Table 1), the condition for the frequency ratio still holds true, thus making possible measurements for sensitive volumes with greater thickness. Furthermore, in the domain of restricted diffusion in porous media, the measurement of the long-limit value of D is important. As is well-known, this parameter is directly related to the surface/volume ratio of the media [19]. It thus makes possible a measurement that no other unilateral NMR sequence can provide.

Declaration of Competing Interest

The authors declare that they have no known competing financial interests or personal relationships that could have appeared to influence the work reported in this paper.

Acknowledgements

This research has been funded by Irstea and the Brittany Region (SAD-volet 1-2017 MONAI, France) and has benefited from access to the PRISM platform (Rennes, France).

References

[1] R.L. Kleinberg, Well logging, in: D.M. Grant, R.K. Harris (Eds.), Encyclopedia of NMR, John Wiley and Sons, New York, 1996, pp. 4960–4969.
[2] A. Gottwald, U. Scheler, Extrusion monitoring of polymer melts using a high-temperature surface-NMR probe macromol, Mater. Eng. 290 (2005) 438–442.
[3] S. Sharma, F. Casanova, W. Wache, A.L. Segre, B. Blümich, Analysis of historical porous building materials by the NMR-MOUSE, Magn. Reson. Imaging. 21 (2003) 249–255.
[4] B. Blümich, J. Perlo, F. Casanova, Mobile single-sided NMR, Prog. Nuclear Magn. Reson. Spectrosc. 52 (2008) 197–269.
[5] N.O. Goga, K. Kremer, B. Blümich, Non-destructive quality control in tire production: the "NMR-MOUSE", GAK Gummi Fasern Kunststoffe. 58 (2) (2005) 104–108.
[6] B.P. Hills, Applications of low-field NMR to food science, Annu. Rep. NMR Spectrosc. 58 (2006) 177–230.
[7] F. Casanova, J. Perlo, NMR in Inhomogeneous Fields, in: F. Casanova, J. Perlo, B. Blümich (Eds.), Singled-Sided NMR, Springer, Heidelberg, 2011, pp. 11–56.
[8] P. Callaghan, Principles of Nuclear Magnetic Resonance Microscopy, Oxford University Press, Oxford, 1991.
[9] D. Duan, C. Ryan, S. Utzuzawa, Y. Song, M. Hürlimann, Effect of off-resonance on T1 saturation recovery measurement in inhomogeneous fields, J. Magn. Reson. 281 (2017) 31–43.
[10] N. Nestlé, B. Walaszek, M. Nolte, Reduced apparent longitudinal relaxation times in slice-selective experiments in strong magnetic field gradients, J. Magn. Reson. 168 (2004) 46–52.
[11] E.E. Sigmund, W.P. Halperin, Hole-burning measurements in high magnetic field gradients, J. Magn. Reson. 163 (2003) 99–104.
[12] C. Schlichter, Principles of Magnetic Resonance, Springer-Verlag, Heidelberg-New York, 1990, p. 598.
[13] D. Hoult, The solution of the bloch equations in the presence of a varying B1 field - an approach to selective pulse analysis, J. Magn. Reson. 35 (1979) 69–86.
[14] J. Crank, The Mathematics of Diffusion, Clarendon Press, Oxford, 1975.
[15] T.T. Nakashima, M.C. Clung RED, Simulation of two-dimensional NMR spectra using product operators in the spherical basis, J. Magn. Reson. 70 (1986) 187–203.
[16] M. Hürlimann, D. Griffin, Spin dynamics of carr-purcell-meiboom-gill-like sequences in grossly inhomogeneous B0 and B1 fields and application to NMR well logging, J. Magn. Resn. 143 (2000) 120–135.
[17] The ARRL Handbook for Radio Communications, published by the American Radio Relay League, Newington, USA, 1990.
[18] M. Holz, S. Heil, A. Sacco, Temperature-dependent self-diffusion coefficient of water and six selected molecular liquids for calibration in accurate 1H NMR PFG measurements, Phys. Chem. Chem. Phys. 2 (2000) 4740–4742.
[19] P.P. Mitra, P.N. Sen, L.M. Schwartz, Short-time behavior of the diffusion coefficient as a geometrical probe of porous media, Phys. Rev. B 47 (1993) 8565–8574.